catalysts

MDPI

Article

The Effect of $AgInS_2$, SnS, CuS_2, Bi_2S_3 Quantum Dots on the Surface Properties and Photocatalytic Activity of QDs-Sensitized TiO_2 Composite

Anna Malankowska [1,*], Daria Kulesza [1], Jakub Sowik [1], Onur Cavdar [1], Tomasz Klimczuk [2], Grzegorz Trykowski [3] and Adriana Zaleska-Medynska [1]

1 Department of Environmental Technology, Faculty of Chemistry, University of Gdansk, 80-308 Gdansk, Poland; darussia01@wp.pl (D.K.); kubsow@interia.pl (J.S.); o.cavdar.897@studms.ug.edu.pl (O.C.); adriana.zaleska-medynska@ug.edu.pl (A.Z.-M.)

2 Department of Solid State Physics, Faculty of Applied Physics and Mathematics, Gdansk University of Technology, 80-233 Gdansk, Poland; tomasz.klimczuk@pg.edu.pl

3 Faculty of Chemistry, Nicolaus Copernicus University, 7 Gagarina str, 87-100 Toruń, Poland; tryki@umk.pl

* Correspondence: anna.malankowska@ug.edu.pl

Received: 5 March 2020; Accepted: 4 April 2020; Published: 7 April 2020

Abstract: The effect of type ($AgInS_2$, SnS, CuS_2, Bi_2S_3) and amount (5, 10, 15 wt%) of quantum dots (QDs) on the surface properties and photocatalytic activity of QDs-sensitized TiO_2 composite, was investigated. $AgInS_2$, SnS, CuS_2, Bi_2S_3 QDs were obtained by hot-injection, sonochemical, microwave, and hot-injection method, respectively. To characterize of as-prepared samples high-resolution transmission electron microscopy (HRTEM), scanning electron microscopy (SEM), X-ray diffraction (XRD), UV-Vis spectroscopy and photoluminescence (PL) emission spectroscopy were applied. The size of $AgInS_2$, SnS, CuS_2, Bi_2S_3 QDs were 12; 2–6; 2–3, and 1–2 nm, respectively. The QDs and QDs-sensitized TiO_2 composites obtained have been tested in toluene degradation under LEDs light irradiation (λ_{max} = 415 nm and λ_{max} = 375 nm). For pristine QDs the efficiency of toluene degradation increased in the order of $AgInS_2$ < Bi_2S_3 < CuS < SnS under 375 nm and $AgInS_2$ < CuS < Bi_2S_3 < SnS under 415 nm. In the presence of TiO_2/SnS QDs_15% composite, 91% of toluene was degraded after 1 h of irradiation, and this efficiency was about 12 higher than that for pristine QDs under 375 nm. Generally, building the TiO_2/$AgInS_2$ and TiO_2/SnS exhibited higher photoactivity under 375 nm than the pristine TiO_2 and QDs which suggests a synergistic effect between QDs and TiO_2 matrix.

Keywords: photocatalysis; TiO_2; quantum dots; metal sulphides; air purification

1. Introduction

Air pollution poses a major threat to public health globally by virtue of its prevalence and emission by various sources. Among these sources, some volatile organic compounds (VOCs) become a prominent problem due to their toxicity even at low concentrations. Moreover, VOCs, along with inorganic oxides, can be transported over long distances producing secondary air pollutants, and can be responsible for acid rain and global warming [1–3]. In this regard, there is a high demand for an efficient, low-cost and eco-friendly technology, which can be implemented for air purification, even at low pollutant concentration levels. Application of solar light induced photocatalysis could be one of the technologies solving these problems [1,4]. Heterogeneous nano-semiconductor photocatalysis (e.g., TiO_2 NPs) is an efficient method facilitating the degradation of air pollutants, inactivation of bacteria, hydrogen production and photoconversion CO_2 into light hydrocarbon [5–8]. The recombination rate of photogenerated electron−hole pairs and the low visible light utilization of TiO_2 limit its applications in these areas. In recent years, there has been significant interest in the

application of metal sulfides (M_xS_y) for wide band semiconductors modification, because of their high charge separation efficiency and narrow band gaps, which possibly enable light harvesting at longer wavelengths [9]. Liu et al. studied the efficiency of $AgInS_2/TiO_2$ heterostructures in 1,2-dichlorobenzene (o-DCB) degradation under visible light [10]. They observed that $AgInS_2/TiO_2$ composites could expand the visible-light response range and greatly decreased the recombination of photogenerated electron−hole pairs in the composites. The degradation of o-DCB for the most active sample reaches about 50% after 8h of irradiation. Jang et al. prepared Ag–SnS–TiO_2 nanocomposite for methylene blue and rhodamine B degradation under simulated sunlight [11]. The photoactivity of the produced photocatalysts was about 2–3 times higher than that of P25. Compared with bare TiO_2 the CuS/TiO_2 [12], CdS/TiO_2 [13–15], SnS/TiO_2 [16], Ag_2S/TiO_2 [17,18], $CuInS_2/TiO_2$ [19–21], Bi_2S_3/TiO_2 [22–24] nanocomposites present a significant improvement on photocatalytic reactions due to the decreasing recombination of electron–hole pairs and the broadened light absorption spectra. However, the metal sulfides commonly employed for TiO_2 modification have been used in nanoparticle sizes and not in quantum dots sizes. Further, it has been shown that the size of metal sulfides (MS) particles can have an impact on its physicochemical and optical properties. Recently, the literature data demonstrated that the decrease in particle size lowers the recombination of the electron-hole pair within the semiconductor particle. Quantum dots (QDs) with particles size in range from 2 to 20 nm exhibit distinctive properties owing to their high surface-to-volume ratio [25]. Band gap tailoring of QDs is contingent by controlling particle size. Thus, light absorption range and the energy of charge carriers can be modulated. So far, QDs decorated semiconductors particles have aroused attention due to high charge separation efficiency and quantum confinement effects of QDs. To date, the CdS QDs-decorated semiconductors NPs [26–30] a mostly investigated in photocatalytic reaction, but CdS QDs are not stable in the water splitting reaction, which are known to be toxic. Moreover, the use of CdS is restricted due to photocorrosion. To date, metal sulfides quantum dot (MS QDs)-sensitized TiO_2 were not often studied in air purification process. Mazierski et al. synthesized the Ag NPs/Bi_2S_3 QDs/TiO_2 nanotubes (NTs) with the improved photocatalytic efficiency in phenol and toluene degradation which was assigned to the notably increased the electron−hole separation/transfer and synergistic effect between the ordered structure of TiO_2 NTs and the well-distributed Pt NPs and Bi_2S_3 QDs [31]. However, other types of composites, e.g., C QDs/Bi_2WO_6 NPs [32], N-doped C QDs/TiO_2 NPs [33], CdTe QDs/$KTaO_3$ NPs [34], CdTe QDs/$SrTiO_3$ NPs [35], CdTe QDs/$SrTiO_3$ NPs [35] were investigated in pollutants degradation in the gas phase.

Based on the above considerations, this paper focuses on the synthesis methods, surface properties and photocatalytic activity of MS QDs and MS QDs-decorated TiO_2 composites. Herein, a series of non-toxic quantum dots (e.g., $AgInS_2$, SnS, CuS_2, Bi_2S_3) have been applied to investigate the effect of QD typeand amount (5, 10, 15 wt%) on the activity of obtained QDs-TiO_2 hybrids. The proposed hybrid systems are discussed with respect photoactivity in air purification process in the presence of low-powered and low-cost irradiation sources (LEDs λ_{max} = 415 nm and λ_{max} = 375 nm), which reduce the costs of photocatalytic processes.

2. Results and Discussion

Sample labeling, preparation method and photocatalytic activity of prepared QDs and QDs-sensitized TiO_2 are given in Table 1. Initially, we investigated the effect type ($AgInS_2$, SnS, CuS_2, Bi_2S_3) and amount of QDs (5, 10, 15 wt%) on the optical properties and efficiency of toluene degradation in the gas phase using the LEDs.

Table 1. Sample label, preparation method and photocatalytic activity of prepared photocatalysts.

Sample Label	Loading of QDs (wt%)	Preparation Method	Toluene Degradation after 1 h Irradiation (%)	
			λ_{max} = 415 nm	λ_{max} = 375 nm
TiO_2 NPs	0	hydrothermal	45.1	79.1
$AgInS_2$	0	hot-injection	56.2	59.3
$TiO_2/AgInS_2$_5	5	adsorption/calcination	71.1	78.6
$TiO_2/AgInS_2$_10	10	adsorption/calcination	70.7	86.3
$TiO_2/AgInS_2$_15	15	adsorption/calcination	56.1	89.2
SnS	0	sonochemical	14.8	6.50
TiO_2/SnS_5	5	adsorption/calcination	13.7	87.9
TiO_2/SnS_10	10	adsorption/calcination	34.6	79.9
TiO_2/SnS_15	15	adsorption/calcination	36.6	91.1
CuS	0	microwave	25.9	28.1
TiO_2/CuS_5	5	adsorption/calcination	24.7	37.3
TiO_2/CuS_10	10	adsorption/calcination	36.5	46.3
TiO_2/CuS_15	15	adsorption/calcination	40.2	45.6
Bi_2S_3	0	hot-injection	21.8	35.2
TiO_2/Bi_2S_3_5	5	adsorption/calcination	29.8	56.3
TiO_2/Bi_2S_3_10	10	adsorption/calcination	29.7	52.5
TiO_2/Bi_2S_3_15	15	adsorption/calcination	34.7	49.4

2.1. Morphology

To determine the morphology of the obtained TiO_2, scanning electron microscopy (SEM) and high-resolution transmission electron microscopy (HRTEM) images have been performer (Figure 1). As clearly shown, TiO_2 showed an irregular particles and porous surface morphology. The average size of TiO_2 was in the range of 100−800 nm.

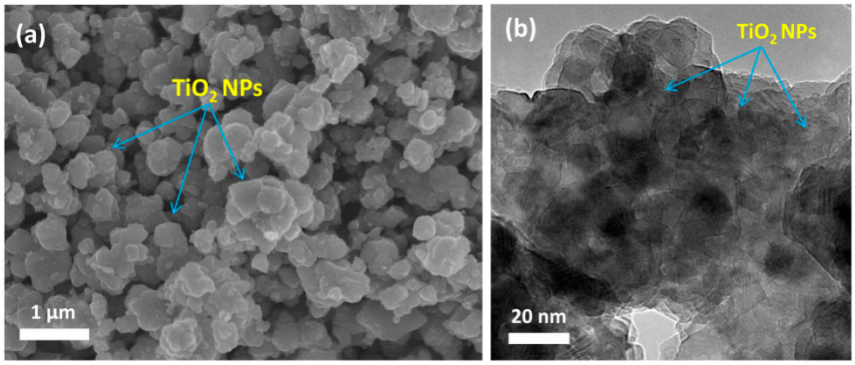

Figure 1. (**a**) SEM and (**b**) HR-TEM images for TiO_2 NPs.

The HRTEM measurements were performer to characterize the morphology of obtained QDs (Figure 2). The average size of $AgInS_2$ QDs was about 12 nm (Figure 2a). However, the accurate size of $AgInS_2$ QDs was difficult to determine, due to the presence of an amorphous layer, indicating the presence of oleic acid, 1-octadecene, dodecanethiol and oleylamine (used during the synthesis) on surface of $AgInS_2$ QDs QDs (Figure 2b). As clearly shown SnS QDs were small in size and have spherical shape with average size from 2 to 6 nm (after 15 min. in ultrasonic bath) (Figure 2c–d). Cheraghizade et al. obtained SnS QDs by applying different sonication times of 10, 15, and 20 min. They observed that the sizes of the SnS QDs decreased from 7.15 to 3.66 nm with the times of sonication were enhanced [36]. Based on Figure 1e–f, the average size of CuS QDs obtained by microwave method

during 9 min. were in the range of 2–3 nm. Chaudhary et al. also obtained CuS QDs with size of 2–3 nm in 2 min using microwave and water as medium [37]. The Figure 2g–h clearly shows very small Bi_2S_3 quantum dots embedded on the surface of TiO_2 NPs. Bi_2S_3 QDs were spherical with size in the range of 1–2 nm. In addition, Table S1 presents the transmission electron microscopy energy-dispersive X-ray spectroscopy (TEM-EDX) analysis. These results show the combination of QDs and the TiO_2 NPs which have resulted in the formation of heterojunction structure between these two components. Furthermore, this composed interaction between TiO_2 and QDs may play an crucial role in accelerating the separation of the photogenerated charge carriers [34,38].

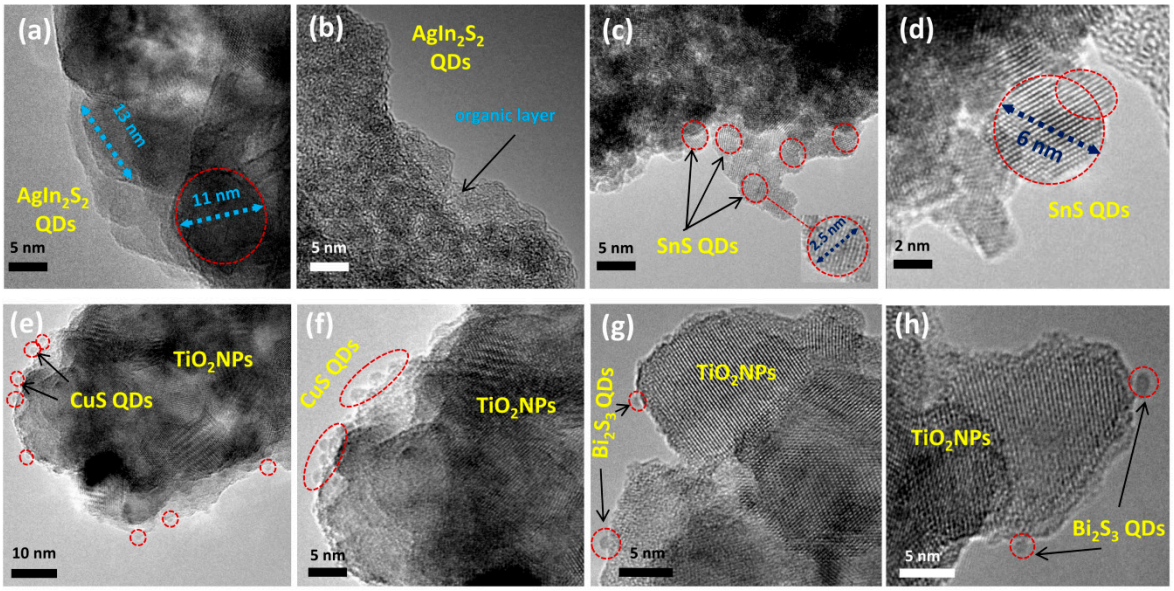

Figure 2. HR-TEM images for (**a**,**b**) $AgInS_2$ QDs, (**c**,**d**) SnS QDs, (**e**,**f**) TiO_2/CuS_15 QDs, and (**g**,**h**) TiO_2/Bi_2S_3_15 QDs.

2.2. UV-Vis Spectra

The optical properties for all prepared photocatalysts were investigated by UV–vis spectra analysis with the wavelength from 250 to 650 nm (Figure 3). The characteristic sharp edge was observed at 390–400 nm which is in agreement with the intrinsic band-gap absorption of anatase TiO_2 (3.2eV). For $AgInS_2$ the onset of absorption peak was observed at 600 nm with a maximum at 450 nm (Figure 3a). All TiO_2 modified with $AgInS_2$ QDs exhibit enhanced absorption in the visible light spectrum, in comparison with the pure TiO_2. Furthermore, the increased absorption in the visible range with increasing amount (from 5 to 15%) of $AgInS_2$ QDs can be seen. It is worth mentioning that the highest amount of $AgInS_2$ QDs (15 wt%) onto TiO_2 surface led to induced absorption in range from 400 to 650 nm. Therefore, these results confirm that QDs have been successfully combined with the TiO_2 NPs and the heterojunctions in the fabricated composites were formed. Significantly widened absorption spectrum into the visible region has been achieved by introducing SnS QDs onto TiO_2 NPs, due to the photosensitizing effect of the incorporated SnS QDs with TiO_2 NPs matrix (Figure 3b). For TiO_2 modified with CuS QDs, it can also be seen that the absorbance peaks were shifted to longer wavelengths, compared with pristine TiO_2 (Figure 3c). The bare SnS QDs and CuS QDs have shown remarkable absorption in both the UV and visible regions. No significant effect was observed on absorption properties by coupling TiO_2 NPs with the black colored Bi_2S_3 QDs in comparison to pristine TiO_2 [24]. (Figure 3d).

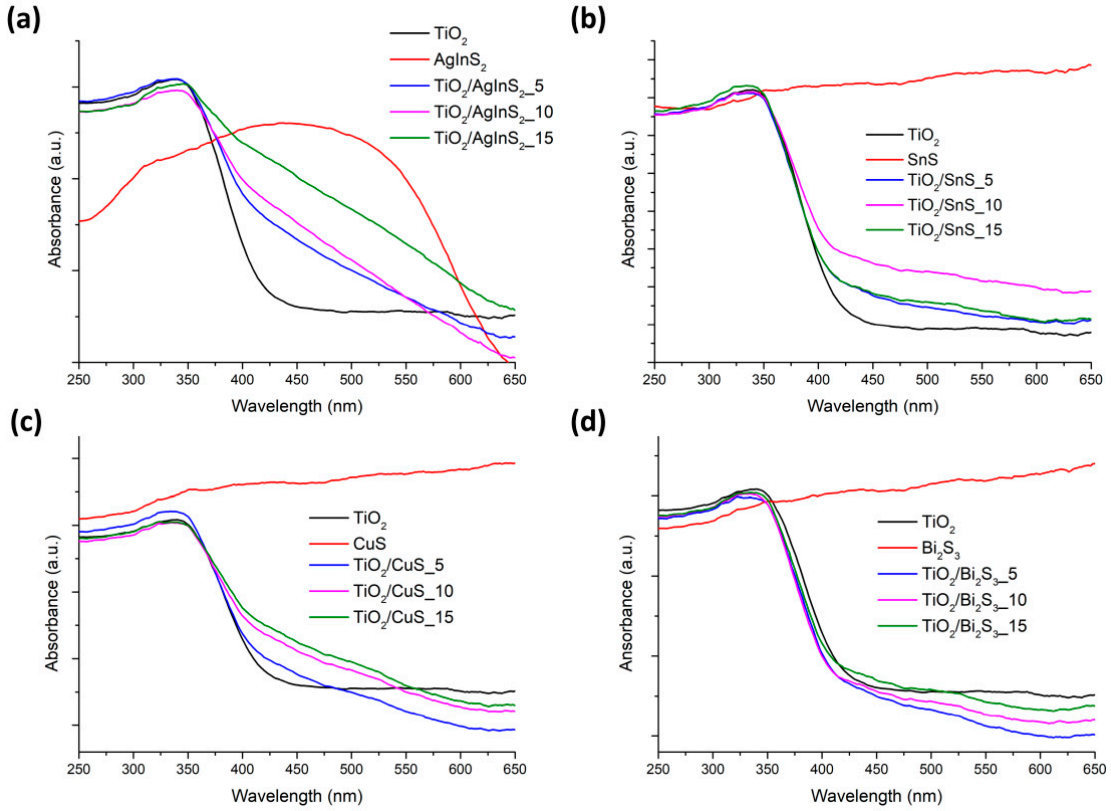

Figure 3. UV-Vis spectra for (**a**) TiO_2, $AgInS_2$ and TiO_2 modified with $AgInS_2$ (5, 10, 15 wt%), (**b**) TiO_2, SnS and TiO_2 modified with SnS (5, 10, 15 wt%), (**c**) TiO_2, CuS_2 and TiO_2 modified with CuS (5, 10, 15 wt%), (**d**) TiO_2, Bi_2S_3 and TiO_2 modified with Bi_2S_3 (5, 10, 15 wt%).

2.3. Photoluminescence Properties

It is essential to study the photoluminescence (PL) emission spectra of semiconductor photocatalysis, which can provide information regarding electron-hole recombination processes. The PL signal is obtained from emitted photons by electron-hole pair recombination in a photocatalysis [39].The higher PL emission signal the more efficient the recombination process, and the lower the activity for photocatalysis [40]. Figure 4 displays PL emission spectra of prepared photocatalysts at an excitation wavelength of 330 nm. Pristine TiO_2 exhibited the highest PL intensity due to its low separation efficiency. PL spectra of anatase TiO_2 materials are attributed to three kinds of physical origins: Self-trapped excitons (420 nm), oxygen vacancies (420, 440 and 455) and surface states/defects (480, 522 nm) [39]. The emission around 480 nm has been observed for all prepared samples, which can be attributed to the charge transfer from Ti^{3+} to oxygen anion in a TiO_6^{8-} complex associated with oxygen vacancies at the surface [41,42]. The maximum of emission band of $AgInS_2$ QDs synthesized by hot-injection method at 130°C for 6 min is located around 650 nm (Figure 4a). Along with the increase in the $AgInS_2$ QDs content, the PL intensity dropped down and achieved its lowest level at 15 wt% QDs content, suggesting the highest separation and transfer efficiency of photogenerated electron-hole pairs. Among the TiO_2/SnS and TiO_2/ Bi_2S_3 photocatalysts, the lowest PL was observed for the sample containing 10 wt% of QDs (Figure 4b,d). Based on a comparison of changes in PL intensity of all TiO2 modified with CuS, it can be observed that the luminescence intensity decreased with increasing amount of CuS QDs (Figure 4c). Considering these results, the proposed QDs can raise the effective separation of the photogenerated electrons and holes in TiO_2/QDs heterojunction, thus promoting the charge separation and improving the photocatalytic performance.

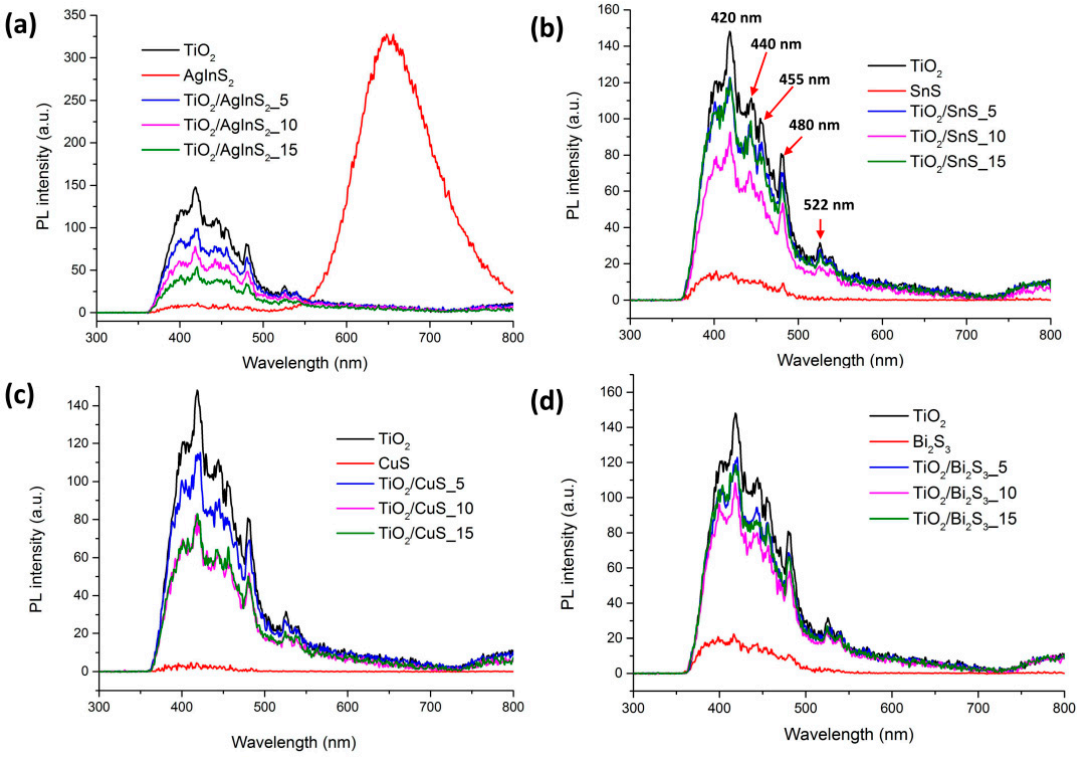

Figure 4. PL spectra of (**a**) TiO_2, $AgInS_2$ and TiO_2 modified with $AgInS_2$ (5, 10, 15 wt%), (**b**) TiO_2, SnS and TiO_2 modified with SnS (5, 10, 15 wt%), (**c**) TiO_2, CuS_2 and TiO_2 modified with CuS (5, 10, 15 wt%), (**d**) TiO_2, Bi_2S_3 and TiO_2 modified with Bi_2S_3 (5, 10, 15 wt%).

2.4. XRD Analysis

Figure 5 shows the X-ray diffraction (XRD) patterns of pristine TiO_2, QDs and TiO_2/QDs_15 composites. The peak diffraction observed at the 2θ values of 25, 37.8, 48.1, and 53.9° can be assigned to (101), (004), (200), and (105) crystallographic plane of anatase TiO_2 with tetragonal crystal structure [31,43]. Three peaks at 2θ values of 26.5, 44.7, and 52.3° corresponding to the (112), (220), and (312) indices of the tetragonal crystal structure of $AgInS_2$ QDs, respectively (Figure 5a) [44]. The broad diffraction peaks show the fine grains of the $AgInS_2$ QDs. Orthorhombic structured SnS QDs is identified from the XRD pattern in Figure 5b. Three peaks at 2θ values of 25.9, 31.48 and 44.4° corresponds to planes (120), (111) and (141) [45]. For CuS QDs peaks around 27.7, 29.3, 31.8, and 47.9° can be assigned to the corresponding (100), (102), (103) and (110) crystal planes of CuS, which can be indexed as a hexagonal structure [46] (Figure 5c). The diffraction peaks that were matched to the orthorhombic structure of Bi_2S_3 QDs can be observed (Figure 5d) [47]. The very broad diffraction peaks show the fine grains of the Bi_2S_3 QDs. After loading 15 wt% of QDs, the XRD patterns of the QDs-sensitized TiO_2 composite were almost the same as that of pure TiO_2 confirming that surface modification did not influence the crystalline properties of TiO_2.

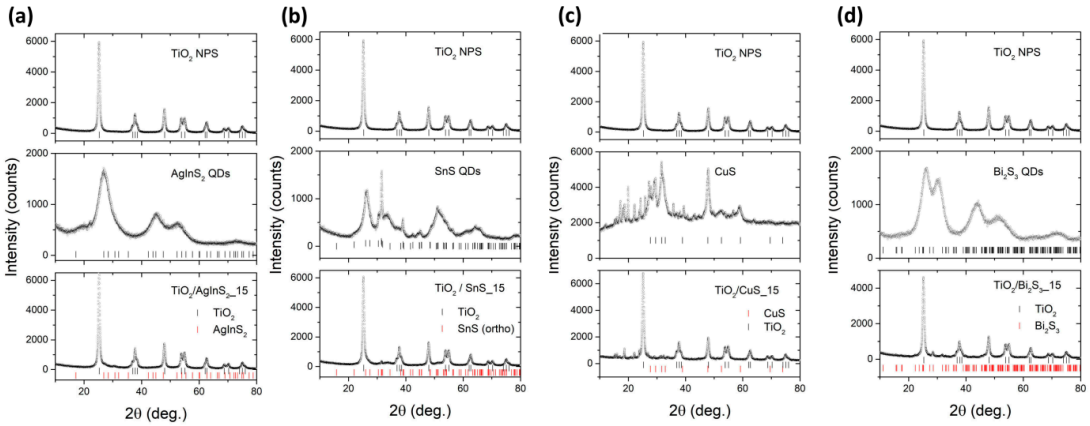

Figure 5. XRD analysis for (**a**) TiO_2, $AgInS_2$ and TiO_2/$AgInS_2$_15, (**b**) TiO_2, SnS and TiO_2/SnS_15, (**c**) TiO_2, CuS_2 and TiO_2/CuS_15, (**d**) TiO_2, Bi_2S_3 and TiO_2/Bi_2S_3_15.

2.5. FT-IR Analysis

Figure 6 shows fourier transform infrared (FT-IR) spectra for pure TiO_2 NPs, pure QDs and for TiO_2 modified with 15% weight of selected sulphide. The groups of very weak, sharp bands occurring at wave numbers above 3600 cm^{-1} and 1600–1800 cm^{-1} are attributed to water vapor. Likewise strong doublet at 2336 cm^{-1} clearly comes from carbon dioxide, exactly from O=C=O stretching vibrations [48]. Mentioned above both compounds are contaminations that may have been present at measurement chamber during the analysis.

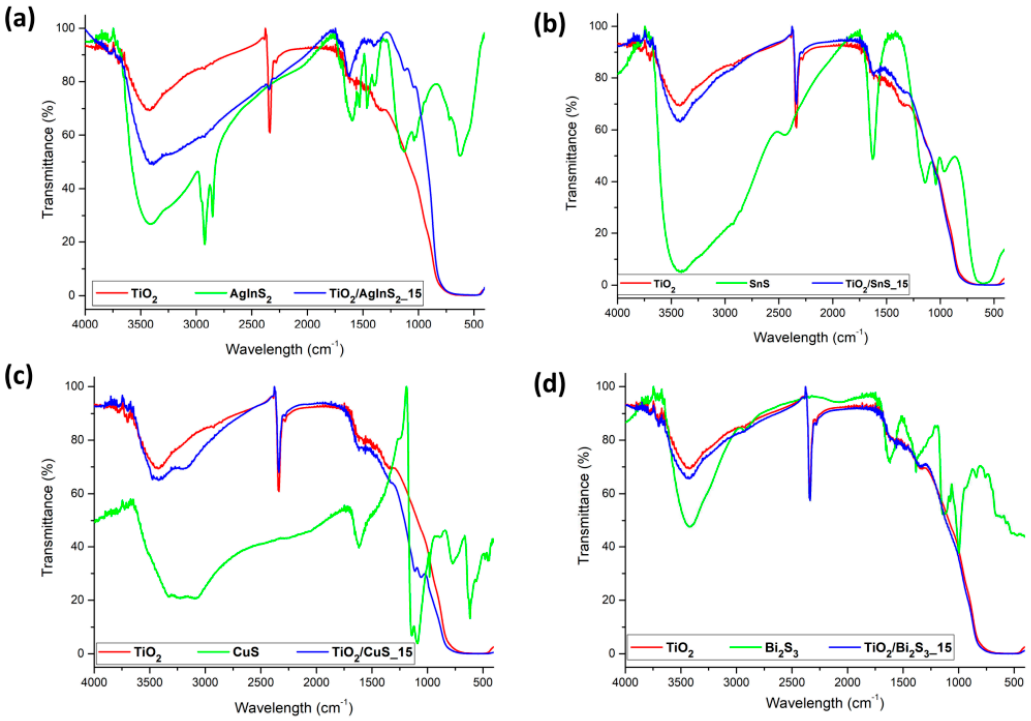

Figure 6. FT-IR spectra for QDs and TiO_2 modified by (**a**) TiO_2, $AgInS_2$ and TiO_2/$AgInS_2$_15, (**b**) TiO_2, SnS and TiO_2/SnS_15, (**c**) TiO_2, CuS_2 and TiO_2/CuS_15, (**d**) TiO_2, Bi_2S_3 and TiO_2/Bi_2S_3_15.

Furthermore CO_2 can be adsorbed on the surface of TiO_2 NPs as the case band is very distinct. The FTIR spectrum of pure TiO_2 was given in Figure 6 a–d (red line) is characterized by several bands, which are evidence of the presence of specific functional groups. A very broad absorption band, centered in 3420 cm^{-1}, originates from O–H stretching vibrations from hydroxyl groups of molecules

surface. Medium band at 1620 cm^{-1} corresponds to water bending vibrations [49]. These two bands are repeated in most of the spectra presented in this chapter. Whereas peak at 1370 cm^{-1} and the strongest flat region between 400–850 cm^{-1} are typical for Ti–O and Ti–O–Ti stretching oscillation [50]. FT-IR $AgInS_2$ spectra are given at Figure 6a. A strong pronounced doublet observed at 2923 and 2853 cm^{-1} are attributed to symmetric and asymmetric stretching modes of C–H [51]. Absorption, in this case, is strong because oleic acid (OA) was used to preparation probe therefore long chain hydrocarbon fragments were introduced. Bands at 1590, 1530 and twice peaks 1464, 1393 cm^{-1} corresponding to C=O stretching, N–H and H–C–H bending vibrations, respectively. The above bands are evidence of the presence of amide or amine groups that can form next bonds, two peaks at 1135 and 1032 cm^{-1} are attributed to C–N stretching modes. It confirms the existence of amide functional groups [44]. Strong peaks at 722 and 630 cm^{-1} are the result of H–C–H rocking and C–S stretching oscillation, respectively. $TiO_2/AgInS_2$_15 is the only case in which the shape of the spectrum is clearly closer to the shape of the pure $AgInS_2$ than the TiO_2 spectra. Each peak described for the $AgInS_2$ is also visible in the spectrum of modified TiO_2, the only exceptions are the peaks in the range 500–700 cm^{-1}. Also, the sharp, strong absorption band visible on every spectrum at 2336 cm^{-1} (attributed to CO_2) has been reduced in the $TiO_2/AgInS_2$ chart. The above analysis demonstrates that, in this case, the absorption $AgInS_2$ on the surface of TiO_2 occurred with the highest efficiency in this publication. At Figure 6b was presented spectra TiO_2 modified with tin(II) sulphide. Namely bands at SnS spectra in 613, 950–1150 and 2440 cm^{-1} are typical for this compound [52,53]. Strengthened signal for 1620 cm^{-1} results from overlapping water and N-H bending vibrations amine group becomes from ammonium used in synthesis of semiconductor [54]. TiO_2/SnS_15 spectrum exhibit features of both components although at first it seems identical to pure TiO_2 NPs. Transmittance at wave numbers corresponding to characteristic bands of SnS is reduces which is visible as subtle peaks. Wavy spectra between 950–1150 cm^{-1} and slight signal at 2440 cm^{-1} are evidence of an effective adsorption process, SnS on TiO_2 surface. CuS spectra are given at Figure 6c peak obtained for CuS in 3090 cm^{-1} comes from functional groups on surface of semiconductor, exactly N–H stretching vibrations. Two very strong vibrations at 1140 and 1090 cm^{-1} corresponds to C–O and S–O stretching [8]. These three bands described above are also visible in the TiO_2/CuS_15 spectrum. Furthermore, oscillation localized between 500–700 cm^{-1} are typical for Cu–S stretching and are only clearly visible in the CuS spectra [55,56]. In Figure 6d was shown the effect of TiO_2 modification using Bi_2S_3. The most important peaks are situated under 1500 cm^{-1}, namely, a sharp band at 1390 cm^{-1} is due to the complex Bi^{3+} and citrate anions, which results from the type of precursors used for synthesis. Strong, sharp peaks at 1150 and 1000 cm^{-1} are attributed to stretching asymmetric and symmetric O–S–O vibrations. The band characteristics for Bi appear in the range 400–600 cm^{-1} [57]. All bands described above, except those in the range 400–600 cm^{-1}, are reflected in spectra of TiO_2/Bi_2S_3_15. Waved lines were observed in corresponding to interpreted peaks. Invisible bands in the 400–600 cm^{-1} range are masked by very strong, broad absorption band of TiO_2. A similar phenomenon occurs in all spectra in this paragraph.

2.6. Photocatalytic Activity in the Gas Phase

In order to investigate the photocatalytic activity of obtained photocatalysts, photocatalytic degradation of toluene in the gas phase were studied under 375 and 415 nm light irradiation. Under 375 nm for pristine QDs the efficiency of toluene degradation increased in the order of $AgInS_2$ < Bi_2S_3 < CuS < SnS. All samples containing SnS quantum dots boosted the photocatalytic activity of TiO_2 NPs under 375 nm light irradiation (Table 1, Figure 7). Cheraghizade et al. showed that SnS QDs photocatalytic activity depends on particle size. Prolonged sonication-assisted synthesis results in smaller crystallite size SnS QDs with higher photocatalytic activity. This is due to the reduced size of SnS QDs, in which the ratio of surface-to-volume is enhanced and so electron-hole creation of samples are also increased [36]. Although, pristine SnS QDs had very low activity in toluene photodegradation, the application of SnS QDs onto TiO_2 surface most boosted reaction yield. The TiO_2/SnS_15 sample exhibited the highest performance among other photocatalysts with 91.1% toluene

degradation after 1 hour irradiation under 375 nm which proves that the load of 15% SnS QDs on TiO_2 NPs matrix improved the photocatalytic activity of bare TiO_2 NPs and pristine QDs by 1.15, and 12 times, respectively. High efficiency toluene degradation was also observed for TiO_2/SnS_5 and TiO_2/SnS_10, i.e., 87.9 and 79.7% of toluene was degraded after 1 h under 375 nm, respectively. These SnS QDs, when decorated onto the surfaces of TiO_2 enable precise engineering of the band structure of the obtained composite. Through decoration of SnS QDs of suitable sizes, the charge separation of the TiO_2 NPs is improved, while maintaining a suitable electronic potential to generate extra oxidizing species for toluene degradation [58]. High toluene degradation was observed for TiO_2/$AgInS_2$_10 and TiO_2/$AgInS_2$_15, while 5% modification (TiO_2/$AgInS_2$_5) decreased the activity of TiO_2 NPs under 375 nm. Generally, it was observed, that in case of TiO_2/$AgInS_2$ composites, enhancement of concentration (from 5 to 15 wt.%) resulted in a linear increase of photoactivity under 375 nm and clear decrease in the recombination of electron hole pairs. The efficiency of toluene degradation increased from 78.6; 86.3 to 89.2% for TiO_2/$AgInS_2$_5, TiO_2/$AgInS_2$_10, and TiO_2/$AgInS_2$_15, respectively. The optimal content of quantum dots for TiO_2/CuS composites was 10 wt.%. After 1 h, 46.3% toluene was degraded in the presence of TiO_2/CuS_10 under 375 nm. Further increase in CuS QDs concentration (to 15 wt.%) resulted in a slight drop of photoactivity to 45.6 % for the sample TiO_2/CuS_15. The TiO_2/Bi_2S_3_5 sample exhibited the highest performance among TiO_2/ Bi_2S_3 composites under 375 nm (56.3%). Further increase in Bi_2S_3 concentration (to 15 wt.%) resulted in a drop of photoactivity to 49.4% for the sample TiO_2/ Bi_2S_3_15. Lin et al. [59] reported that in case of $CdSnO_3$-decorated CdS nanowire, for 2.5 at% of $CdSnO_3$ the highest charge carrier separation was observed. Generally, building the TiO_2/$AgInS_2$ and TiO_2/SnS composite resulted in a synergistic effect between QDs and TiO_2 matrix. It was also observed that increasing $AgInS_2$ QDs content on the surface TiO_2 NPs resulted in (*i*) improved light harvesting ability, (*ii*) reduced recombination of e-h pairs and (*iii*) improved photoactivity under UV irradiation. Whereas modification with CuS and Bi_2S_3 showed lowered the activity than pristine TiO_2 but higher activity than pristine CuS and Bi_2S_3 QDs under 375 and 415 nm. Under 415 nm for pristine QDs the efficiency of toluene degradation increased in the order of $AgInS_2$ < CuS < Bi_2S_3 < SnS. An increase in SnS and CuS QDs concentration (from 5 to 15 wt.%) caused a linear increase in photoactivity under 415 nm. However, the highest toluene degradation was observed by $AgInS_2$ modified TiO_2 NPs while other modifications decreased the activity of TiO_2 NPs after 1 h under 415 nm. TiO_2/$AgInS_2$_5 had the higher photocatalytic activity compare to TiO_2/$AgInS_2$_10 and TiO_2/$AgInS_2$_15 with 71.1% toluene degradation (Table 1, Figure 7). Therefore, it can be suggested that the most active sample for toluene degradation adheres to the type of the light irradiation. This is probably due to the electronic band structure of the TiO_2 NPs and quantum dots that affect the photoexcited electrons and holes transfer route in the photocatalysts [21,60]. In summary, the photocatalytic activity was dependent on (i) type of QDs, (ii) amount of QDs and (iii) wavelength of the light irradiation.

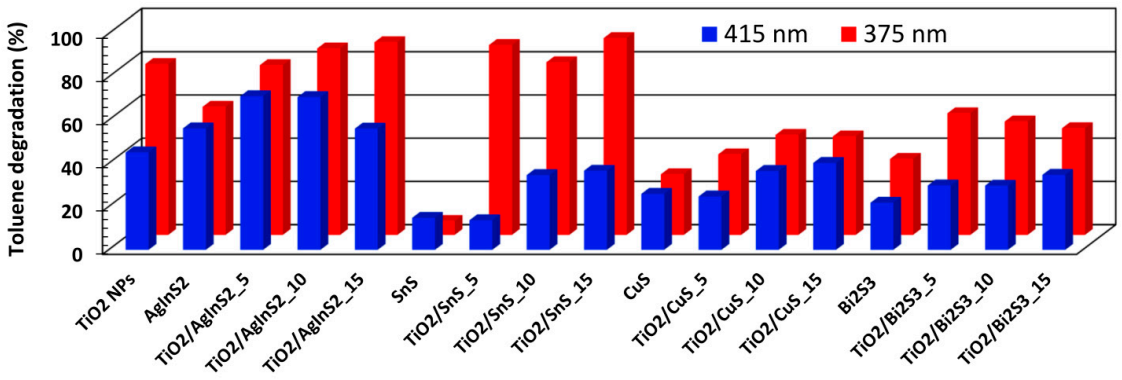

Figure 7. Photocatalytic activities of obtained photocatalysts for toluene photodegradation after 1 h irradiation of LEDs λ_{max} = 375 nm and λ_{max} = 415 nm.

In addition to those, the photostability of the most active sample under 375 nm irradiation, TiO_2/SnS_15, was tested by carrying out 4 subsequent cycles. At the end of the cycle, the activity of TiO_2/SnS_15 diminished by 9.65% (Figure 8). This deactivation can be explained mainly by the partial oxidation of toluene that leads to formation of intermediates such as benzaldehyde, benzyl alcohol, benzoic acid, benzene, and phenol which remain on the photocatalysis surface by strong adsorption [61]. In particular, with benzoic acid intermediate, more carbonyl group arises on the photocatalysis surface, which inhibits the electron density of the benzyl ring that makes the benzyl ring more inert, thus hard to break it [62,63].

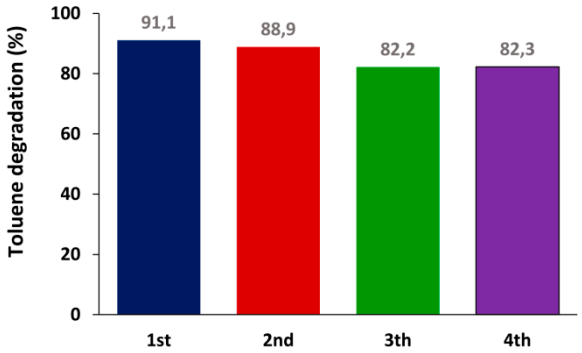

Figure 8. Photostability of TiO_2/SnS_15% measured in the fourth subsequent cycles in the toluene degradation reaction in the presence of LED λ_{max} = 375 nm.

The photocatalytic mechanism for QDs-sensitized TiO_2 composite under visible and UV irradiation has been proposed (Figure 9). All tested non-toxic QDs has narrow band gap and more negative conduction band (CB) energy level than CB of TiO_2 (Table 2).

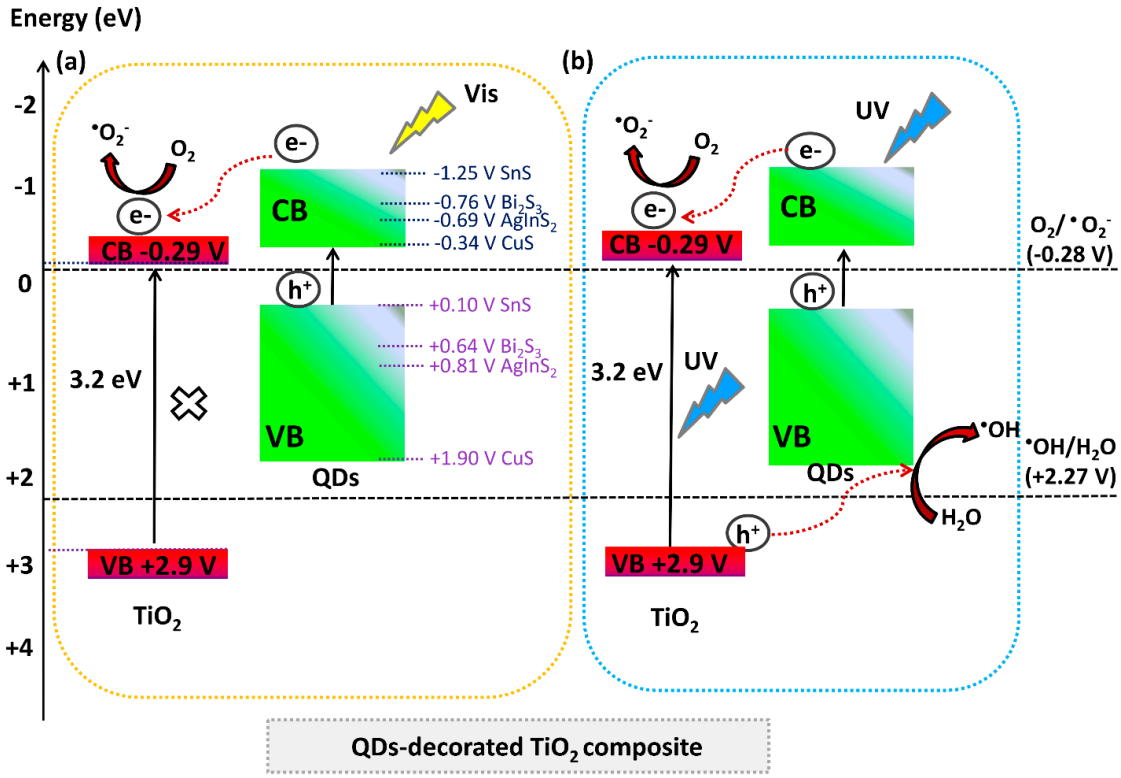

Figure 9. Proposed mechanism of photocatalytic reactions in the presence of QDs-sensitized TiO_2 composite under (**a**) visible, and (**b**) UV irradiation.

Table 2. Band gap values and positions of the VB and CB for tested samples.

Type of Sample	Band Gap Eg (eV)	Position of VB (V)	Position of CB (V)	Ref.
TiO_2 NPs	3.2	+2.9	−0.29	[64]
$AgInS_2$ QDs	1.5	+0.81	−0.69	[65]
SnS QDs	1.35	+0.1	−1.25	[66]
CuS QDs	2.25	+1.9	−0.34	[67]
Bi_2S_3 QDs	1.4	+0.64	−0.76	[31]

Photoexcited electrons are generated on the CB of QDs in upon the visible light absorption that leaves holes in the VB (Figure 9a). Since the CB of TiO_2 is more positive than the CB of QDs, the photoexcited electrons transfer from the photoexcited QDs into the CB of TiO_2 expectedly. Those electrons in CB of TiO_2 reduce the O_2 adsorbed on the surface of the photocatalyst to form $^{\bullet}O_2^-$. The VB potentials of QDs are more negative than the redox potential of $^{\bullet}OH/H_2O$ (+2.27 V), indicating that the holes in the VB of QDs cannot oxidize H_2O to produce $^{\bullet}OH$.

Under UV irradiation, both TiO_2 NPs and QDs was excited (Figure 9b). The electron from QDs can be inject into the CB of TiO_2 NPs. The electron transfer from QDs to the TiO_2 NPs is determined by the energy difference between the two CB positions energy levels, which acts as a driving force for interparticle electron transfer [25,68]. The highest difference between the CB positions energy levels were observed for TiO2 and SnS QDs, which means fastest electron transfer from QDs to TiO2 NPs and a high photocatalytic activity of those composites as showed in the experimental section. While, the holes formed in the VB of TiO_2 had oxidative potential and can be easily transferred to the VB of QDs and then oxidize H_2O and ^{-}OH to produce $^{\bullet}OH$. In this way, the photogenerated electron-holes pairs can be effectively separated, which results in higher photoactivity in particular in presence of $TiO_2/AgInS_2$ and TiO_2/SnS composite.

3. Experimental

3.1. Materials and Instruments

Tetrabutyl titanate (TBT, 97%, Sigma Aldrich, Saint Louis, MO, USA) and glycerol (99.5%, POCH, Gliwice, Poland) were used for TiO_2 NPs prepartion. Silver nitrate ($AgNO_3$, 99%, Sigma Aldrich, Saint Louis, MO, USA), indium (III) acetylacetonate ($In(acac)_3$, 99.99%, Sigma Aldrich, Saint Louis, MO, USA), sulfur powder (S, 99.98%, POCH, Gliwice, Poland), 1-octadecene (ODE, 90%, Sigma Aldrich, Saint Louis, MO, USA), dodecanethiol (DDT, 98%, Alfa Aesar, Haverhill, MA, USA), oleylamine (OLA, 90%, ACROS ORGANICS, Gell Belgium), oleic acid (OA, 90%, Sigma Aldrich, Saint Louis, MO, USA) were used for $AgInS_2$ QDs synthesis. Tin chloride ($SnCl_2$, 99%, POCH, Gliwice, Poland), ammonium acetate (CH_3COONH_4, 99%, Sigma Aldrich, Saint Louis, MO, USA), ammonia (NH_3, 25%, Chempur, Piekary Śląskie, Poland) sodium thiosulfate ($Na_2S_2O_3x5H_2O$, 99,5%, POCH, Gliwice, Poland) were used for SnS QDs synthesis. Thioacetamide (C_2H_5NS, 99%, Sigma Aldrich, Saint Louis, MO, USA), copper chloride ($CuCl_2xH_2O$, 99%, POCH, Gliwice, Poland) were used for CuS QDs synthesis. Sodium sulfide (Na_2S, 99.9%, Sigma Aldrich, Saint Louis, MO, USA), ammonium bismuth citrate (99%, Sigma Aldrich, Saint Louis, MO, USA), starch ($C_6H_{12}O_5$, pure p.a.) were used for Bi_2S_3 QDs synthesis. Deionized water was used in all the experiments.

The UV−vis spectra of samples were recorded in the scan range 250−650 nm using UV−vis spectrophotometer (UV 2600, Shimadzu, Kioto, Japan) equipped with $BaSO_4$ as the reference. The photoluminescence (PL) emission spectra were measured by a PerkinElmer Luminescence Spectrometer LS 50B (Hamamatsu, Japan) equipped with xenon discharge lamp as an excitation source. The samples were excited with 330 nm at room temperature and the emission was scanned between 300 and 800 nm. X-ray diffraction (X'Pert Pro MPD Philips diffractometer, Almelo, The Netherands) with Cu Kα radiation λ = 1.5418 Å was used to determine the sample's composition. The measurements

were performed on the 2θ range of 10–80°. The morphology of samples have been analyzed by high-resolution transmission electron microscopy (HRTEM, Brno, Czech Republic, FEI Europe, model TecnaiF20 X-Twin) and scanning electron microscopy (JEOL, Tokyo, Japan, JSM-7610F operating at 15 kV). The preparation of the TEM samples was the following: sonication for 5 seconds of a few milligrams of sample in ethanol (99.8% anhydrous) using ultrasounds, then applying a drop of the solution of 5 µl on a carbon coated copper mesh with holes (Lacey type Cu 400 mesh, Plano), then the solvent was evaporating at room temperature. FT-IR spectra were obtained on a Bruker model IF S66 FTIR spectrometer using potassium bromide discs.

3.2. Sample Preparation

3.2.1. TiO_2 NPs Preparation

The pristine TiO_2 NPs were synthesized by one-step solvothermal method. In a typical procedure, TBT (2.99 g) and glicerol (1.99 g) were mixed with 45 mL absolute ethyl alcohol, respectively. Then, both solutions were mixed together, followed by stirring for 1h. Then obtained suspension was transferred into a Teflon-lined stainless steel autoclave (200 ml capacity) (170 °C for 24 h). After being cooled in the air to room temperature, the products were washed three times with ethanol and then dried in an oven at 80 °C for 24 h. The white TiO_2 powder was calcined at 500°C for 2 h (in air, heating rate of 2 °C/min) (Figure 10).

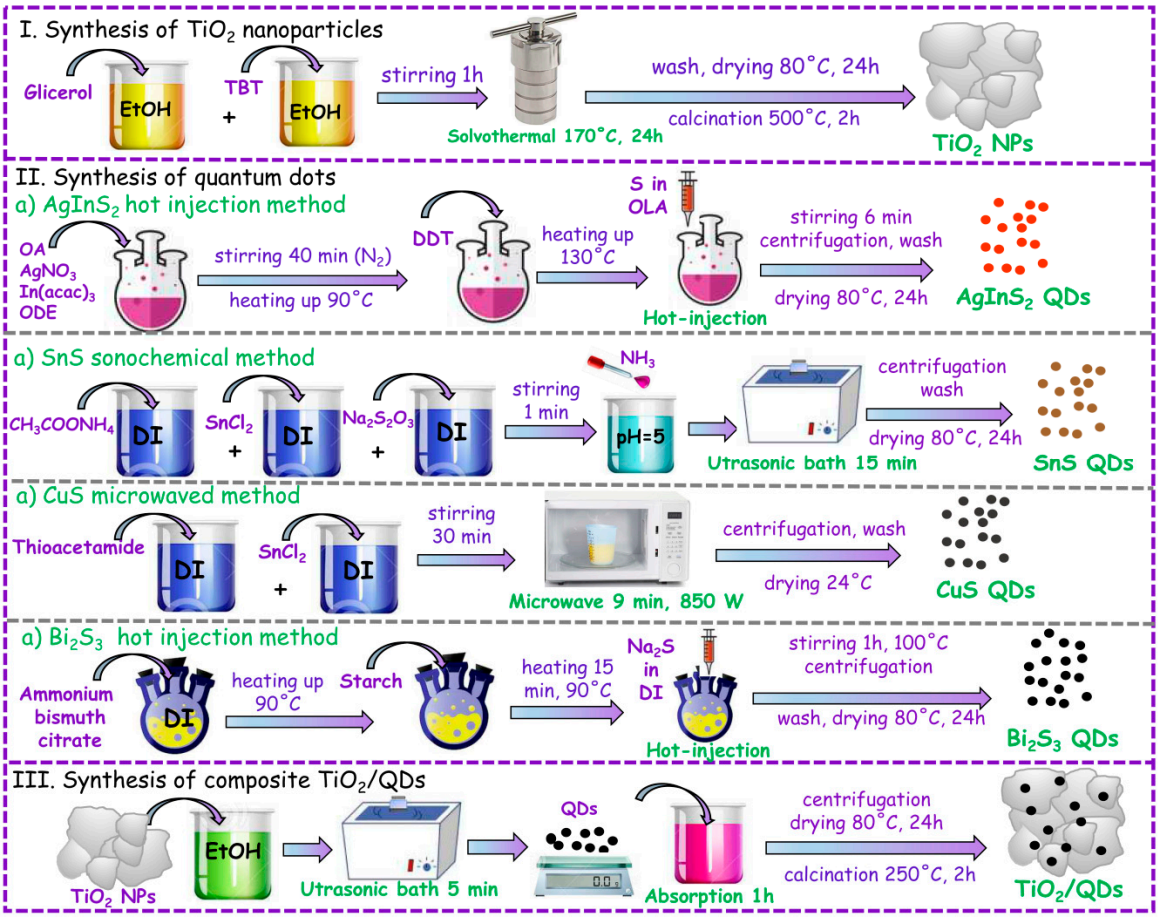

Figure 10. Schematic diagram for the formation of TiO_2, QDs ($AgInS_2$, SnS, CuS, Bi_2S_3) and TiO_2/QDs composite.

3.2.2. Quantum Dots Preparation

(a) $AgInS_2$ QDs Preparation

The $AgInS_2$ QDs were synthesized by hot-injection method similar to that described by Ruan et al. [69]. $AgNO_3$ (0.0176 g), $In(acac)_3$ (0.208 g) and OA (0.47 mL) were mixed and added into a three-neck flask. Then, 8 ml of ODE was added to the obtained solution. The mixing solution was stirred and degassed with N_2 for 40 min. After that, the solution was heated to 90 °C and then DDT (1.0 mL) was injected into the flask. The obtained solution was then heated to 130 °C and the sulfur solution (0.0053 g S powder dissolved in 2.6 mL OLA) was quickly injected, and the solution continued stirring for 6 min. The resulting liqiud product was orange color. After being cooled to room temperature, the products were collected by centrifugation (6000 rpm, 10 min) and washed 3× with ethanol. Finally, the $AgInS_2$ QDs was dried (80 °C for 24 h) (Figure 10).

(b) SnS QDs Preparation

The SnS QDs were synthesized by sonochemical method [36]. In a first step, three solutions were prepared (*i*) $SnCl_2$ x $2H_2O$ (0.9165 g) in 40 ml deionized water (DI), (*ii*) ammonium acetate (0.3119 g) in 40 ml DI, and (*iii*) $Na_2S_2O_3$ (0.9578 g) dissolved in 20 ml DI. Then, all above solutions were mixed at 25 °C, followed by stirring for 1 minute and its pH was adjusted at 5 using addition of ammonia. After that the reaction mixture was introduced into an ultrasonic bath for 15 min. The products were washed times with deionized water, centrifuged (10 min. 6000 rpm) and dried (80 °C for 24 h). The resulting product was brown color (Figure 10).

(c) CuS QDs Preparation

The CuS QDs were prepared by through a simple and cost-effective microwave method [37]. In a typical procedure, $CuCl_2$ x $2H_2O$ (0.1344 g dissolved in 100 mL H_2O) and thioacetamide (0.0901 g dissolved in 100 ml H_2O) were mixed for 30 min at 25 °C. Then, the resulting solution was placed into the microwave 9 min at 850 W and the formation of black precipitates appeared. The CuS QDs were collected by centrifugation (6000 rpm, 20 min), washed 3 times with DI and dried at 25 °C (Figure 10).

(d) Bi_2S_3 QDs Preparation

Bi_2S_3 QDs were obtained by the hot-injection method using a starch capping agent [68]. Firstly, ammonium bismuth citrate (0.4043 g) was dissolved in 20 ml DI. Then mixture was heated to 95 °C and soluble starch (0.2015 g) was added and was kept at 95 °C for about 15 min. Then, the Na_2S (0.4051 g dissolved in 20 mL of deionized water) was added into to the ammonium bismuth citrate solution and stirred at 100 °C for 1 h. The powder was collected by centrifugation (6000 rpm, 10 min), and washed 3× with DI. Finally, the Bi_2S_3 QDs was dried at 80 °C for 24 h (Figure 10).

3.2.3. Preparation of Quantum Dot-sensitized TiO_2 Composites

TiO_2/QDs ($AgInS_2$, CuS, SnS, Bi_2S_3) photocatalysts were synthesized by absorption method (Figure 10). Typically, 30 mL of ethanol containing the TiO_2 NPs was ultrasonicated for 5 min to make NPs completely dispersed. Then, a different amount of QDs (5,10,15% wt%) was added to suspension of photocatalysts, followed by stirring for 6 h (250 rpm/min.). After that, TiO_2/QDs photocatalysts were collected by centrifugation (7000 rpm, 20 min) and dried at 70 °C for 24 h. Finally, the powder was calcined at 250 °C for 2 h (in air, heating rate of 3 °C/min). The description of the as-prepared photocatalysts is shown in Table 1.

3.3. Measurement of Photocatalytic Activity

The photocatalytic activity was determined in the toluene degradation process [70]. As an irradiation source, an array of 25 LEDs (λ_{max} = 375 nm, 13.16 mW/cm^2) and (λ_{max} = 415 nm, 1.6 mW/cm^2) (Optel, Opole, Poland), these diodes contain a part of UV radiation) were used. In a typical procedure, a thin film of the photocatalyst was prepared by suspending of photocatalyst (0.01 g) in water and loading it on a glass plate (3 cm × 3 cm) by painting technique. The gas mixture (with toluene concentration 200 ppm) was passed through the photoreactor (1 min), and the reactor was

kept in the dark for 30 min in order to achieve equilibrium. The toluene concentration was determined by using a GC (TRACE 1300, Thermo Scientific, Waltham, MA, USA, FID, Elite-5 capillary column).

4. Conclusions

In summary, for pristine QDs the efficiency of toluene degradation increased in the order of $AgInS_2$ < Bi_2S_3 < CuS < SnS under 375 nm and $AgInS_2$ < CuS < Bi_2S_3 < SnS under 415 nm. All samples containing SnS quantum dots boosted the photocatalytic activity of TiO_2 NPs under 375 nm light irradiation, which are related to a heterojunction with highest difference between the CB positions energy levels and thus faster electron transfer from SnS QDs to TiO_2 NPs. The loading of 15% SnS QDs on TiO_2 NPs matrix improved the photocatalytic activity of bare QDs 12 times. Generally, building the TiO_2/$AgInS_2$ and TiO_2/SnS exhibited higher photoactivity under 375 nm than the pristine TiO_2 and QDs, which resulted in a synergistic effect between QDs and TiO_2 matrix. This enhancement can be also related with the improved light harvesting ability and decreasing recombination of electron–hole pairs by QDs-decorated TiO_2. Whereas, modification with CuS and Bi_2S_3 showed lowered the activity than pristine TiO_2 but higher activity than pristine CuS and Bi_2S_3 QDs under 375 and 415 nm. The photocatalytic activity of pristine QDs and QDs-decorated TiO_2 composites is different, which means that it is important to create the appropriate heterojunction between QDs and semiconductor nanoparticles. Our results may provide useful guide for designing of QDs-sensitized TiO_2 composite for the air purification in the presence of low powered and low cost irradiation sources (LEDs), which reduce the costs of the photocatalytic processes. QD-decorated semiconductor NPs composites are considered to play an increasing role in photocatalytic applications in the near future.

Supplementary Materials: The following are available online at http://www.mdpi.com/2073-4344/10/4/403/s1, **Table S1.** TEM-EDX analysis for (a) $AgInS_2$ QDs, (b) SnS QDs, (c) TiO_2/$AgInS_2$_15, (d) TiO_2/SnS_15, (e) TiO_2/CuS_15, (f) TiO_2/Bi_2S_3_15.

Author Contributions: Conceptualization, A.M.; funding acquisition, A.M; experiment design, A.M., D.K., J.S., O.C., T.K. and G.T.; data analysis, A.M., J.S., O.C., A.Z-M., T.K. and G.T.; writing—original draft, A.M., J.S., O.C., T.K. and A.Z.-M.; writing—review and editing, A.M. and A.Z.-M.; supervision, A.M. All authors have read and agreed to the published version of the manuscript.

Funding: This research was financially supported by Polish National Science Centre (Grant Sonata, No. NCN 2016/23/D/ST8/02682).

Conflicts of Interest: The authors declare no conflict of interest.

References

1. Bajorowicz, B.; Kobylański, M.P.; Malankowska, A.; Mazierski, P.; Nadolna, J.; Pieczyńska, A.; Zaleska-Medynska, A. 4—Application of metal oxide-based photocatalysis. In *Metal Oxide-Based Photocatalysis*; Zaleska-Medynska, A., Ed.; Elsevier: Amsterdam, The Netherlands, 2018; pp. 211–340.
2. Nath, R.K.; Zain, M.F.M.; Jamil, M. An environment-friendly solution for indoor air purification by using renewable photocatalysts in concrete: A review. *Renew. Sustain. Energy Rev.* **2016**, *62*, 1184–1194. [CrossRef]
3. Ren, H.; Koshy, P.; Chen, W.-F.; Qi, S.; Sorrell, C.C. Photocatalytic materials and technologies for air purification. *J. Hazard. Mater.* **2017**, *325*, 340–366. [CrossRef] [PubMed]
4. Wang, X.; Wang, F.; Sang, Y.; Liu, H. Full-Spectrum Solar-Light-Activated Photocatalysts for Light–Chemical Energy Conversion. *Adv. Energy Mater.* **2017**, *7*, 1700473. [CrossRef]
5. Gao, C.; Low, J.; Long, R.; Kong, T.; Zhu, J.; Xiong, Y. Heterogeneous Single-Atom Photocatalysts: Fundamentals and Applications. *Chem. Rev.* **2020**. [CrossRef] [PubMed]
6. Kampouri, S.; Stylianou, K.C. Dual-Functional Photocatalysis for Simultaneous Hydrogen Production and Oxidation of Organic Substances. *ACS Catal.* **2019**, *9*, 4247–4270. [CrossRef]
7. Wang, Z.; Li, C.; Domen, K. Recent developments in heterogeneous photocatalysts for solar-driven overall water splitting. *Chem. Soc. Rev.* **2019**, *48*, 2109–2125. [CrossRef]
8. Byrne, C.; Subramanian, G.; Pillai, S.C. Recent advances in photocatalysis for environmental applications. *J. Environ. Chem. Eng.* **2018**, *6*, 3531–3555. [CrossRef]

9. Di, T.; Xu, Q.; Ho, W.; Tang, H.; Xiang, Q.; Yu, J. Review on Metal Sulphide-based Z-scheme Photocatalysts. *ChemCatChem* **2019**, *11*, 1394–1411. [CrossRef]
10. Liu, B.; Li, X.; Zhao, Q.; Ke, J.; Tadé, M.; Liu, S. Preparation of $AgInS_2/TiO_2$ composites for enhanced photocatalytic degradation of gaseous o-dichlorobenzene under visible light. *Appl. Catal. B Environ.* **2016**, *185*, 1–10. [CrossRef]
11. Jiang, Y.; Yang, Z.; Zhang, P.; Jin, H.; Ding, Y. Natural assembly of a ternary Ag–SnS–TiO_2 photocatalyst and its photocatalytic performance under simulated sunlight. *RSC Adv.* **2018**, *8*, 13408–13416. [CrossRef]
12. Chandra, M.; Bhunia, K.; Pradhan, D. Controlled Synthesis of CuS/TiO_2 Heterostructured Nanocomposites for Enhanced Photocatalytic Hydrogen Generation through Water Splitting. *Inorg. Chem.* **2018**, *57*, 4524–4533. [CrossRef] [PubMed]
13. Kaur, A.; Umar, A.; Anderson, W.A.; Kansal, S.K. Facile synthesis of CdS/TiO_2 nanocomposite and their catalytic activity for ofloxacin degradation under visible illumination. *J. Photochem. Photobiol. A Chem.* **2018**, *360*, 34–43. [CrossRef]
14. Al-Fahdi, T.; Al Marzouqi, F.; Kuvarega, A.T.; Mamba, B.B.; Al Kindy, S.M.Z.; Kim, Y.; Selvaraj, R. Visible light active $CdS@TiO_2$ core-shell nanostructures for the photodegradation of chlorophenols. *J. Photochem. Photobiol. A Chem.* **2019**, *374*, 75–83. [CrossRef]
15. Yang, H.; Liu, Z.; Wang, K.; Pu, S.; Yang, S.; Yang, L. A Facile Synthesis of TiO_2–CdS Heterostructures With Enhanced Photocatalytic Activity. *Catal. Lett.* **2017**, *147*, 2581–2591. [CrossRef]
16. Zhang, X.; Gao, Y.; Nengzi, L.-C.; Li, B.; Gou, J.; Cheng, X. Synthesis of SnS/TiO_2 nano-tube arrays photoelectrode and its high photoelectrocatalytic performance for elimination of 2,4,6-trichlorophenol. *Sep. Purif. Technol.* **2019**, *228*, 115742. [CrossRef]
17. Yadav, S.K.; Jeevanandam, P. Synthesis of Ag_2S–TiO_2 nanocomposites and their catalytic activity towards rhodamine B photodegradation. *J. Alloys Compd.* **2015**, *649*, 483–490. [CrossRef]
18. Li, Z.; Xiong, S.; Wang, G.; Xie, Z.; Zhang, Z. Role of Ag_2S coupling on enhancing the visible-light-induced catalytic property of TiO_2 nanorod arrays. *Sci. Rep.* **2016**, *6*, 19754. [CrossRef] [PubMed]
19. Xu, F.; Zhang, J.; Zhu, B.; Yu, J.; Xu, J. $CuInS_2$ sensitized TiO_2 hybrid nanofibers for improved photocatalytic CO_2 reduction. *Appl. Catal. B Environ.* **2018**, *230*, 194–202. [CrossRef]
20. Li, C.; Xi, Z.; Fang, W.; Xing, M.; Zhang, J. Enhanced photocatalytic hydrogen evolution activity of $CuInS_2$ loaded TiO_2 under solar light irradiation. *J. Solid State Chem.* **2015**, *226*, 94–100. [CrossRef]
21. Shen, F.; Que, W.; Liao, Y.; Yin, X. Photocatalytic Activity of TiO_2 Nanoparticles Sensitized by $CuInS_2$ Quantum Dots. *Ind. Eng. Chem. Res.* **2011**, *50*, 9131–9137. [CrossRef]
22. Kim, J.; Kang, M. High photocatalytic hydrogen production over the band gap-tuned urchin-like Bi_2S_3-loaded TiO_2 composites system. *Int. J. Hydrog. Energy* **2012**, *37*, 8249–8256. [CrossRef]
23. Lu, J.; Han, Q.; Wang, Z. Synthesis of TiO_2/Bi_2S_3 heterojunction with a nuclear-shell structure and its high photocatalytic activity. *Mater. Res. Bull.* **2012**, *47*, 1621–1624. [CrossRef]
24. Yang, L.; Sun, W.; Luo, S.; Luo, Y. White fungus-like mesoporous Bi_2S_3 ball/TiO_2 heterojunction with high photocatalytic efficiency in purifying 2,4-dichlorophenoxyacetic acid/Cr(VI) contaminated water. *Appl. Catal. B Environ.* **2014**, *156*, 25–34. [CrossRef]
25. Bajorowicz, B.; Kobylański, M.P.; Gołąbiewska, A.; Nadolna, J.; Zaleska-Medynska, A.; Malankowska, A. Quantum dot-decorated semiconductor micro- and nanoparticles: A review of their synthesis, characterization and application in photocatalysis. *Adv. Colloid Interface Sci.* **2018**, *256*, 352–372. [CrossRef] [PubMed]
26. Zhu, Y.; Wang, Y.; Chen, Z.; Qin, L.; Yang, L.; Zhu, L.; Tang, P.; Gao, T.; Huang, Y.; Sha, Z.; et al. Visible light induced photocatalysis on CdS quantum dots decorated TiO_2 nanotube arrays. *Appl. Catal. A Gen.* **2015**, *498*, 159–166. [CrossRef]
27. Liu, L.; Hui, J.; Su, L.; Lv, J.; Wu, Y.; Irvine, J.T.S. Uniformly dispersed CdS/CdSe quantum dots co-sensitized TiO_2 nanotube arrays with high photocatalytic property under visible light. *Mater. Lett.* **2014**, *132*, 231–235. [CrossRef]
28. Li, X.; Wang, J.; Men, Y.; Bian, Z. TiO_2 mesocrystal with exposed (001) facets and CdS quantum dots as an active visible photocatalyst for selective oxidation reactions. *Appl. Catal. B Environ.* **2016**, *187*, 115–121. [CrossRef]
29. Ge, L.; Liu, J. Synthesis and photocatalytic performance of novel CdS quantum dots sensitized Bi_2WO_6 photocatalysts. *Mater. Lett.* **2011**, *65*, 1828–1831. [CrossRef]

30. Mao, L.; Jiang, W.; He, L.; Fang, P. Photocatalytic activity of TiO_2 sensitized by CdS quantum dots under visible-light irradiation. *Wuhan Univ. J. Nat. Sci.* **2011**, *16*, 313–318. [CrossRef]
31. Mazierski, P.; Nadolna, J.; Nowaczyk, G.; Lisowski, W.; Winiarski, M.J.; Klimczuk, T.; Kobylański, M.P.; Jurga, S.; Zaleska-Medynska, A. Highly Visible-Light-Photoactive Heterojunction Based on TiO_2 Nanotubes Decorated by Pt Nanoparticles and Bi_2S_3 Quantum Dots. *J. Phys. Chem. C* **2017**, *121*, 17215–17225. [CrossRef]
32. Qian, X.; Yue, D.; Tian, Z.; Reng, M.; Zhu, Y.; Kan, M.; Zhang, T.; Zhao, Y. Carbon quantum dots decorated Bi_2WO_6 nanocomposite with enhanced photocatalytic oxidation activity for VOCs. *Appl. Catal. B Environ.* **2016**, *193*, 16–21. [CrossRef]
33. Martins, N.C.T.; Ângelo, J.; Girão, A.V.; Trindade, T.; Andrade, L.; Mendes, A. N-doped carbon quantum dots/TiO_2 composite with improved photocatalytic activity. *Appl. Catal. B Environ.* **2016**, *193*, 67–74. [CrossRef]
34. Bajorowicz, B.; Nadolna, J.; Lisowski, W.; Klimczuk, T.; Zaleska-Medynska, A. The effects of bifunctional linker and reflux time on the surface properties and photocatalytic activity of CdTe quantum dots decorated $KTaO_3$ composite photocatalysts. *Appl. Catal. B Environ.* **2017**, *203*, 452–464. [CrossRef]
35. Marchelek, M.; Grabowska, E.; Klimczuk, T.; Lisowski, W.; Zaleska-Medynska, A. Various types of semiconductor photocatalysts modified by CdTe QDs and Pt NPs for toluene photooxidation in the gas phase under visible light. *Appl. Surf. Sci.* **2017**, *393*, 262–275. [CrossRef]
36. Cheraghizade, M.; Jamali-Sheini, F.; Yousefi, R.; Niknia, F.; Mahmoudian, M.R.; Sookhakian, M. The effect of tin sulfide quantum dots size on photocatalytic and photovoltaic performance. *Mater. Chem. Phys.* **2017**, *195*, 187–194. [CrossRef]
37. Chaudhary, G.R.; Bansal, P.; Mehta, S.K. Recyclable CuS quantum dots as heterogeneous catalyst for Biginelli reaction under solvent free conditions. *Chem. Eng. J.* **2014**, *243*, 217–224. [CrossRef]
38. Cui, W.; An, W.; Liu, L.; Hu, J.; Liang, Y. Novel Cu_2O quantum dots coupled flower-like BiOBr for enhanced photocatalytic degradation of organic contaminant. *J. Hazard. Mater.* **2014**, *280*, 417–427. [CrossRef]
39. Liqiang, J.; Yichun, Q.; Baiqi, W.; Shudan, L.; Baojiang, J.; Libin, Y.; Wei, F.; Honggang, F.; Jiazhong, S. Review of photoluminescence performance of nano-sized semiconductor materials and its relationships with photocatalytic activity. *Solar Energy Mater. Solar Cells* **2006**, *90*, 1773–1787. [CrossRef]
40. Yen, Y.C.; Chen, J.Z.; Lu, Y.J.; Gwo, S.; Lin, K.J. Chain-network anatase/TiO_2 (B) thin film with improved photocatalytic efficiency. *Nanotechnology* **2014**, *25*, 235602. [CrossRef]
41. Grabowska, E.; Marchelek, M.; Klimczuk, T.; Trykowski, G.; Zaleska-Medynska, A. Noble metal modified TiO_2 microspheres: Surface properties and photocatalytic activity under UV–vis and visible light. *J. Mol. Catal. A Chem.* **2016**, *423*, 191–206. [CrossRef]
42. Saraf, L.V.; Patil, S.I.; Ogale, S.B.; Sainkar, S.R.; Kshirsager, S.T. Synthesis of Nanophase TiO_2 by Ion Beam Sputtering and Cold Condensation Technique. *Int. J. Mod. Phys. B* **1998**, *12*, 2635–2647. [CrossRef]
43. Gołąbiewska, A.; Malankowska, A.; Jarek, M.; Lisowski, W.; Nowaczyk, G.; Jurga, S.; Zaleska-Medynska, A. The effect of gold shape and size on the properties and visible light-induced photoactivity of Au-TiO_2. *Appl. Catal. B Environ.* **2016**, *196*, 27–40. [CrossRef]
44. Chang, J.-Y.; Wang, G.-Q.; Cheng, C.-Y.; Lin, W.-X.; Hsu, J.-C. Strategies for photoluminescence enhancement of $AgInS_2$ quantum dots and their application as bioimaging probes. *J. Mater. Chem.* **2012**, *22*, 10609–10618. [CrossRef]
45. Deepa, K.G.; Nagaraju, J. Growth and photovoltaic performance of SnS quantum dots. *Mater. Sci. Eng. B* **2012**, *177*, 1023–1028. [CrossRef]
46. Li, S.; Ge, Z.-H.; Zhang, B.-P.; Yao, Y.; Wang, H.-C.; Yang, J.; Li, Y.; Gao, C.; Lin, Y.-H. Mechanochemically synthesized sub-5nm sized CuS quantum dots with high visible-light-driven photocatalytic activity. *Appl. Surf. Sci.* **2016**, *384*, 272–278. [CrossRef]
47. Ijaz, S.; Ehsan, M.F.; Ashiq, M.N.; He, T. Synthesis of a Bi_2S_3/CeO_2 nanocatalyst and its visible light-driven conversion of CO_2 into CH_3OH and CH_4. *Catal. Sci. Technol.* **2015**, *5*, 5208–5215. [CrossRef]
48. Derric, M.; Stulik, D.; Landry, J. *Infrared Spectroscopy in Conservation Science*; Getty Publications: Los Angeles, CA, USA, 2000.
49. León, A.; Reuquen, P.; Garín, C.; Segura, R.; Vargas, P.; Zapata, P.; Orihuela, A.P. FTIR and Raman Characterization of TiO_2 Nanoparticles Coated with Polyethylene Glycol as Carrier for 2-Methoxyestradiol. *Appl. Sci.* **2017**, *7*, 49. [CrossRef]

50. Mugundan, S.; Rajamannan, B.; Viruthagiri, G.; Shanmugam, N.; Gobi, R.; Praveen, P. Synthesis and characterization of undoped and cobalt-doped TiO_2 nanoparticles via sol–gel technique. *Appl. Nanosci.* **2015**, *5*, 449–456. [CrossRef]
51. Deng, M.; Shen, S.; Wang, X.; Zhang, Y.; Xu, H.; Zhang, T.; Wang, Q. Controlled synthesis of $AgInS_2$ nanocrystals and their application in organic–inorganic hybrid photodetectors. *CrystEngComm* **2013**, *15*, 6443–6447. [CrossRef]
52. Salavati-Niasari, M.; Ghanbari, D.; Davar, F. Shape selective hydrothermal synthesis of tin sulfide nanoflowers based on nanosheets in the presence of thioglycolic acid. *J. Alloys Compd.* **2010**, *492*, 570–575. [CrossRef]
53. Mariappan, R.; Mahalingam, T.; Ponnuswamy, V. Preparation and characterization of electrodeposited SnS thin films. *Optik* **2011**, *122*, 2216–2219. [CrossRef]
54. Zhou, T.; Pang, W.K.; Zhang, C.; Yang, J.; Chen, Z.; Liu, H.K.; Guo, Z. Enhanced Sodium-Ion Battery Performance by Structural Phase Transition from Two-Dimensional Hexagonal-SnS_2 to Orthorhombic-SnS. *ACS Nano* **2014**, *8*, 8323–8333. [CrossRef] [PubMed]
55. Tank, N.S.; Parikh, K.D.; Joshi, M.J. Synthesis and characterization of copper sulphide (CuS) nano particles. *AIP Conf. Proc.* **2017**, *1837*, 040018.
56. Riyaz, S.; Parveen, A.; Azam, A. Microstructural and optical properties of CuS nanoparticles prepared by sol–gel route. *Perspect. Sci.* **2016**, *8*, 632–635. [CrossRef]
57. Salavati-Niasari, M.; Behfard, Z.; Amiri, O.; Khosravifard, E.; Hosseinpour-Mashkani, S.M. Hydrothermal Synthesis of Bismuth Sulfide (Bi_2S_3) Nanorods: Bismuth(III) Monosalicylate Precursor in the Presence of Thioglycolic Acid. *J. Clust. Sci.* **2013**, *24*, 349–363. [CrossRef]
58. Lee, K.T.; Lin, C.H.; Lu, S.Y. SnO_2 quantum dots synthesized with a carrier solvent assisted interfacial reaction for band-structure engineering of TiO_2 photocatalysts. *J. Phys. Chem. C* **2014**, *118*, 14457–14463. [CrossRef]
59. Lin, Y.-F.; Hsu, Y.-J. Interfacial charge carrier dynamics of type-II semiconductor nanoheterostructures. *Appl. Catal. B Environ.* **2013**, *130*, 93–98. [CrossRef]
60. Muñoz-Batista, M.J.; Kubacka, A.; Fernández-García, M. Effect of g-C_3N_4 loading on TiO_2-based photocatalysts: UV and visible degradation of toluene. *Catal. Sci. Technol.* **2014**, *4*, 2006–2015. [CrossRef]
61. Young, C.; Lim, T.M.; Chiang, K.; Scott, J.; Amal, R. Photocatalytic oxidation of toluene and trichloroethylene in the gas-phase by metallised (Pt, Ag) titanium dioxide. *Appl. Catal. B Environ.* **2008**, *78*, 1–10. [CrossRef]
62. Cao, L.; Gao, Z.; Suib, S.L.; Obee, T.N.; Hay, S.O.; Freihaut, J.D. Photocatalytic Oxidation of Toluene on Nanoscale TiO_2 Catalysts: Studies of Deactivation and Regeneration. *J. Catal.* **2000**, *196*, 253–261. [CrossRef]
63. Méndez-Román, R.; Cardona-Martínez, N. Relationship between the formation of surface species and catalyst deactivation during the gas-phase photocatalytic oxidation of toluene. *Catal. Today* **1998**, *40*, 353–365. [CrossRef]
64. Leung, D.Y.C.; Fu, X.; Wang, C.; Ni, M.; Leung, M.K.H.; Wang, X.; Fu, X. Hydrogen Production over Titania-Based Photocatalysts. *ChemSusChem* **2010**, *3*, 681–694. [CrossRef] [PubMed]
65. He, W.; Jia, H.; Yang, D.; Xiao, P.; Fan, X.; Zheng, Z.; Kim, H.-K.; Wamer, W.G.; Yin, J.-J. Composition Directed Generation of Reactive Oxygen Species in Irradiated Mixed Metal Sulfides Correlated with Their Photocatalytic Activities. *ACS Appl. Mater. Interfaces* **2015**, *7*, 16440–16449. [CrossRef] [PubMed]
66. Miyauchi, M.; Shiga, Y.; Srinivasan, N.; Atarashi, D.; Sakai, E. Ubiquitous quantum dot-sensitized nanoporous film for hydrogen production under visible-light irradiation. *Mater. Chem. Phys.* **2015**, *160*, 383–388. [CrossRef]
67. Wang, X.; Li, L.; Fu, Z.; Cui, F. Carbon quantum dots decorated CuS nanocomposite for effective degradation of methylene blue and antibacterial performance. *J. Mol. Liq.* **2018**, *268*, 578–586. [CrossRef]
68. Bajorowicz, B.; Kowalska, E.; Nadolna, J.; Wei, Z.; Endo, M.; Ohtani, B.; Zaleska-Medynska, A. Preparation of CdS and Bi_2S_3 quantum dots co-decorated perovskite-type $KNbO_3$ ternary heterostructure with improved visible light photocatalytic activity and stability for phenol degradation. *Dalton Trans.* **2018**, *47*, 15232–15245. [CrossRef]

69. Ruan, C.; Zhang, Y.; Lu, M.; Ji, C.; Sun, C.; Chen, X.; Chen, H.; Colvin, V.L.; Yu, W.W. White Light-Emitting Diodes Based on $AgInS_2$/ZnS Quantum Dots with Improved Bandwidth in Visible Light Communication. *Nanomaterials* **2016**, *6*, 13. [CrossRef]
70. Malankowska, A.; Kobylański, M.P.; Mikolajczyk, A.; Cavdar, O.; Nowaczyk, G.; Jarek, M.; Lisowski, W.; Michalska, M.; Kowalska, E.; Ohtani, B.; et al. TiO_2 and $NaTaO_3$ Decorated by Trimetallic Au/Pd/Pt Core–Shell Nanoparticles as Efficient Photocatalysts: Experimental and Computational Studies. *ACS Sustain. Chem. Eng.* **2018**, *6*, 16665–16682. [CrossRef]